catalysts

MDPI

Article

Behavior of N-doped TiO_2 and N-doped ZnO in Photocatalytic Azo Dye Degradation under UV and Visible Light Irradiation: A Preliminary Investigation

Olga Sacco [1], Antonietta Mancuso [2], Vincenzo Venditto [1], Stefania Pragliola [1] and Vincenzo Vaiano [2,*]

[1] Department of Chemistry and Biology "A. Zambelli", INSTM Research Unit, University of Salerno, Via Giovanni Paolo II, 132, 84084 Fisciano, SA, Italy
[2] Department of Industrial Engineering, University of Salerno, Via Giovanni Paolo II 132, 84084 Fisciano, SA, Italy
* Correspondence: vvaiano@unisa.it; Tel.: +39-08-996-4340

Abstract: N-doped TiO_2 (N-TiO_2) and N-doped ZnO (N-ZnO) were synthesized utilizing ammonia as a dopant source. The chemico-physical characteristics of synthesized samples were studied by Raman spectroscopy, X-ray diffraction, SEM analysis, N_2 adsorption–desorption at −196 °C, and diffuse reflectance spectroscopy. Compared to undoped samples, the introduction of nitrogen in the semiconductor lattice resulted in a shift of band-gap energy to a lower value: 3.0 eV for N-ZnO and 2.35 eV for N-TiO_2. The photocatalysts were tested for the degradation of Eriochrome Black T (EBT), which was selected as a model azo dye. Both N-doped semiconductors evidenced an improvement in photocatalytic activity under visible light irradiation (62% and 20% EBT discoloration for N-TiO_2 and N-ZnO, respectively) in comparison with the undoped samples, which were inactive in the presence of visible light. Different behavior was observed under UV irradiation. Whereas N-TiO_2 was more photoactive than commercial undoped TiO_2, the introduction of nitrogen in ZnO wurtzite resulted in a drastic reduction in photocatalytic activity, with only 45% EBT discoloration compared to total color removal obtained with the commercial ZnO sample, suggesting intrinsic limitations for doping of this class of semiconductors.

Keywords: N-TiO_2; N-ZnO; photocatalysis; visible light; UV light; Eriochrome Black T dye

check for updates

Citation: Sacco, O.; Mancuso, A.; Venditto, V.; Pragliola, S.; Vaiano, V. Behavior of N-doped TiO_2 and N-doped ZnO in Photocatalytic Azo Dye Degradation under UV and Visible Light Irradiation: A Preliminary Investigation. *Catalysts* **2022**, *12*, 1208. https://doi.org/10.3390/catal12101208

Academic Editor: Xintong Zhang

Received: 31 August 2022
Accepted: 5 October 2022
Published: 10 October 2022

Publisher's Note: MDPI stays neutral with regard to jurisdictional claims in published maps and institutional affiliations.

Copyright: © 2022 by the authors. Licensee MDPI, Basel, Switzerland. This article is an open access article distributed under the terms and conditions of the Creative Commons Attribution (CC BY) license (https://creativecommons.org/licenses/by/4.0/).

1. Introduction

In the last decade, worldwide concerns about environmental and energy-related issues have prompted considerable interest in semiconductor-based heterogeneous photocatalysis [1]. This photocatalytic process can allow sunlight to be used to perform chemical reactions with the aim of degrading highly toxic organic and inorganic substances [2–5], in addition to the selective synthesis of specific organic compounds under mild conditions [6] and the production of solar fuels (such as hydrogen and methane) [7–9]. The most studied semiconductor is TiO_2, although promising results have also been obtained in the presence of ZnO [10,11]. However, an important drawback of TiO_2 and ZnO semiconductors for photocatalysis is that their band gaps are rather large (3.2 eV [12] and 3.4 eV, respectively) making these photocatalysts inactive under visible light (46% of the solar spectrum). To reduce the energy threshold for photoexcitation, a considerable amount of research has been focused on the doping of semiconductors lattice with both transition metals and non-metal elements. The introduction of dopant elements generates energy between the valence and conduction bands of bare semiconductors, leading to suitable modifications of light absorption properties. Among all the dopant elements, N-doped semiconductors seem to be promising photocatalysts that are active under visible light irradiation [13]. In particular, the doping of TiO_2 or ZnO lattice with nitrogen attracted considerable attention because, as reported in the literature [14], the ionic radii of nitrogen and oxygen are similar,

and the energy states of N 2p and O 2p are also similar, with low energy formation. In the case of ZnO, nitrogen is proposed to substitute O sites in the crystalline framework [15], whereas for the TiO_2 crystalline structure, nitrogen doping can result in nitrogen species, such as substitutional or interstitial nitrogen [16]. The possible formation of NO_x species is mostly detected on the surface of semiconductors [17], although the interstitial or substitutional N is preferably present in subsurface layers [17]. Nitrogen has also been reported to simultaneously substitute both O and Ti sites in TiO_2 to form $Ti_{1-y}O_{2-x}N_{x+y}$ instead of $TiO_{2-x}N$ [18]. Various methods have been employed for the incorporation of nitrogen in TiO_2 or ZnO, either based on chemical reactivity (for example, the sol–gel method [15]) or physical methods (for example, magnetron sputtering [19]). The difference seems to lead, at least in some cases, to photocatalytic materials with somewhat differing properties. Therefore, conflicting results have been reported in the literature in this field. Therefore, one of the key aspects that is still under debate is the chemical nature and the location in the semiconductor lattice of the nitrogen species responsible for photoactivity in visible light. However, papers reporting a direct comparison of the photoactivity of N-doped TiO_2 (N-TiO_2) and N-doped ZnO (N-ZnO) are still limited in number. Therefore, in this study, we aim to characterize N-TiO_2 and N-ZnO photocatalysts from a chemico-physical point of view and preliminarily investigate their photocatalytic behavior under UV and visible light irradiation to assess the influence of N species in various semiconductor crystalline hosts on photocatalytic degradation of Eriochrome Black T (EBT) dye, which was selected as a model azo dye. EBT is widely used in complexometric titrations and to dye silk, wool, and nylon [20]. However, EBT is hazardous (carcinogenic) in the event of skin contact and an irritant in the event of eye contact [21].

2. Results and Discussion

2.1. Photocatalyst Characterization

The list of the tested photocatalysts is reported in Table 1.

Table 1. Crystallite size, direct (D) and indirect (I) optical band-gap energy, and specific surface area values of the analyzed photocatalysts.

Sample	N/Ti or N/Zn Nominal Molar Ratio	Crystallite Size, (nm)	Band-Gap (D), (eV)	Band Gap (I), (eV)	Specific Surface Area, ($m^2 \cdot g^{-1}$)
TiO_2	-	17	-	3.3	68
N-TiO_2	18.3	17	-	2.35	45
ZnO	-	25	3.15	-	6
N-ZnO	17.8	33	3.0	-	3

UV-Vis diffuse reflectance spectroscopy (UV-Vis DRS) was employed to study the light absorption properties of all the photocatalysts (Figure 1). Band-gap analysis was performed using the Kubelka–Munk function ($F(R_\infty)$), and the obtained results are shown in Figure 2 and Table 1.

The reflectance spectra of TiO_2 and N-TiO_2 (Figure 1a) essentially differ in terms of the broad absorption in the visible region located in the blue region of electromagnetic radiation (430–480 nm), determining a significant decrease in band-gap values from 3.3 eV (the typical band gap of commercial undoped TiO_2) to 2.35 eV (Figure 2a and Table 1), which is an unexpected value for bare TiO_2 in the anatase phase. The intensity and width of this absorption depend on the preparation method used for synthesis, as reported by di Valentin et al. [17]. Nevertheless, the spectrum of N-TiO_2 is very close to that reported by other authors who synthetized N-doped TiO_2 with different methods [22,23]. On the other hand, the optical absorbance behavior of N-ZnO changed slightly with respect to the commercial sample, indicating that doping alters the optical behavior of N-ZnO to a lesser extent than doping of TiO_2 with nitrogen. A small decrease in band-gap energy of N-ZnO (3.0 eV) was observed with respect to commercial undoped ZnO (3.15 eV) (Figure 2b

and Table 1), suggesting that the energetic intermediate levels generated between the conduction and valence bands of ZnO do not drastically change the band gap value [24].

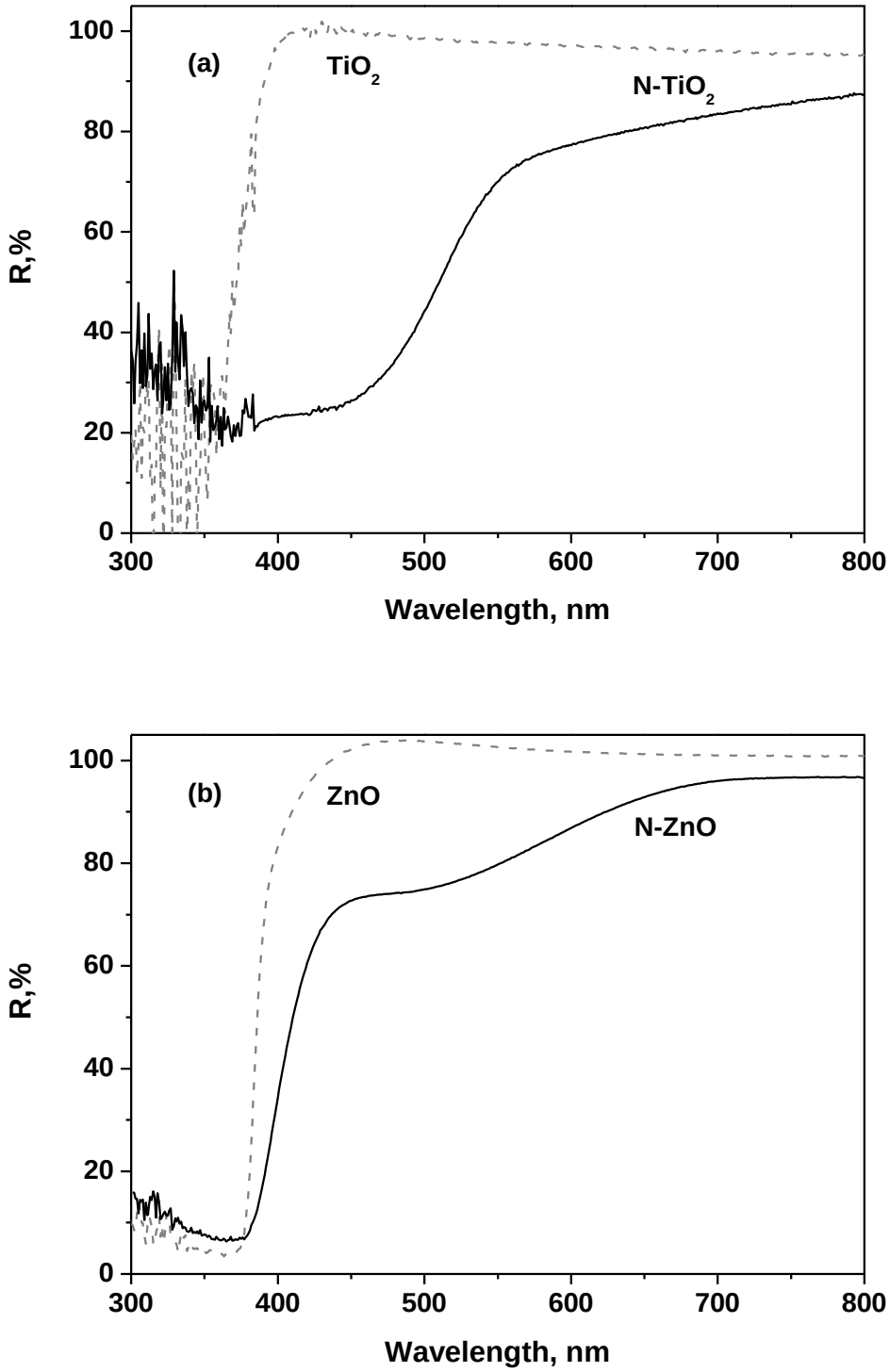

Figure 1. UV-Vis DRS spectra for (**a**) TiO_2 and N-TiO_2, as well as (**b**) ZnO and N-ZnO samples.

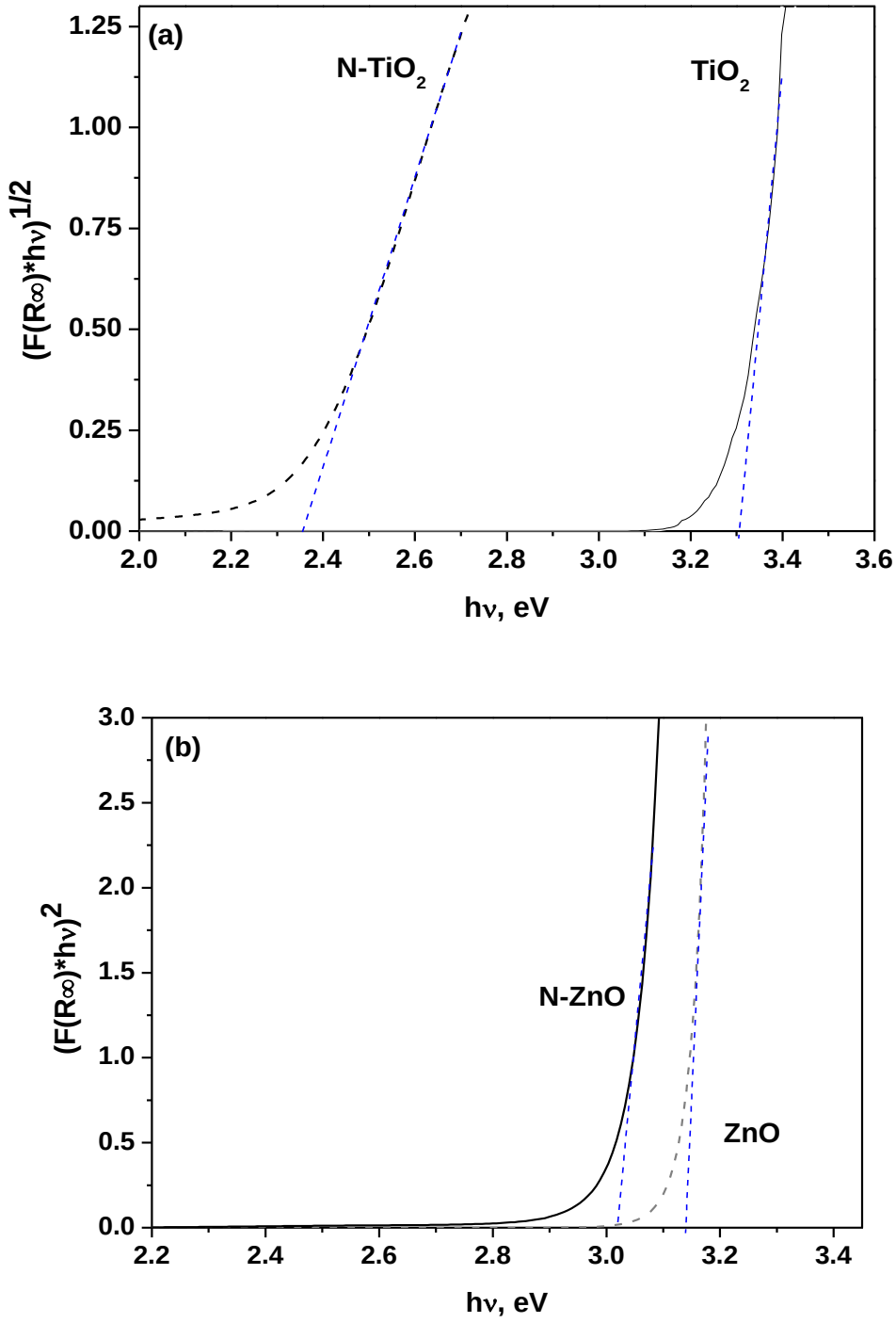

Figure 2. Band-gap estimation for (**a**) TiO_2 and N-TiO_2, as well as (**b**) ZnO and N-ZnO samples.

Raman spectroscopic analysis was employed to examine the possible variations in Raman active vibrational modes of TiO_2 and ZnO due to the presence N into the host lattice (Figure 3). For both TiO_2 and N-TiO_2 samples (Figure 3a), all the signals can be assigned to the Raman active modes of the anatase crystal phase [25,26]. Moreover, a slight blue shift of the Raman active mode ($E_{g(1)}$) was observed from 144 to 146 cm^{-1} for the doped sample, clearly indicating the presence of a nonstoichiometric TiO_{2-x} phase [27,28]. For both ZnO and N-ZnO spectra (Figure 3b), a prominent peak was detected at 438 cm^{-1}, which was associated with the Raman-active dominant mode (E_2(H)) of wurtzite ZnO [29]. Furthermore, two less intense Raman bands were observed at 330 and 378 cm^{-1} and assigned to E_2(H)–E_2(L) (multi-phonon) and A_1 (TO) modes of wurtzite ZnO, respectively [30]. The N-ZnO

sample showed three additional broad and weak signals at 275, 504, and 644 cm^{-1} [31]. It has been argued that the presence of these Raman signals is associated with the presence of nitrogen in the ZnO crystalline framework [31,32]. For the N-ZnO sample, the intensity of the Raman band at 580 cm^{-1} was stronger than that of the commercial ZnO. According to the available literature on doped ZnO photocatalysts [33–35], such a band is due to the presence of oxygen vacancies, the presence of which is increased by the introduction of the dopant element into the ZnO lattice, affecting the stoichiometry of the host semiconductor.

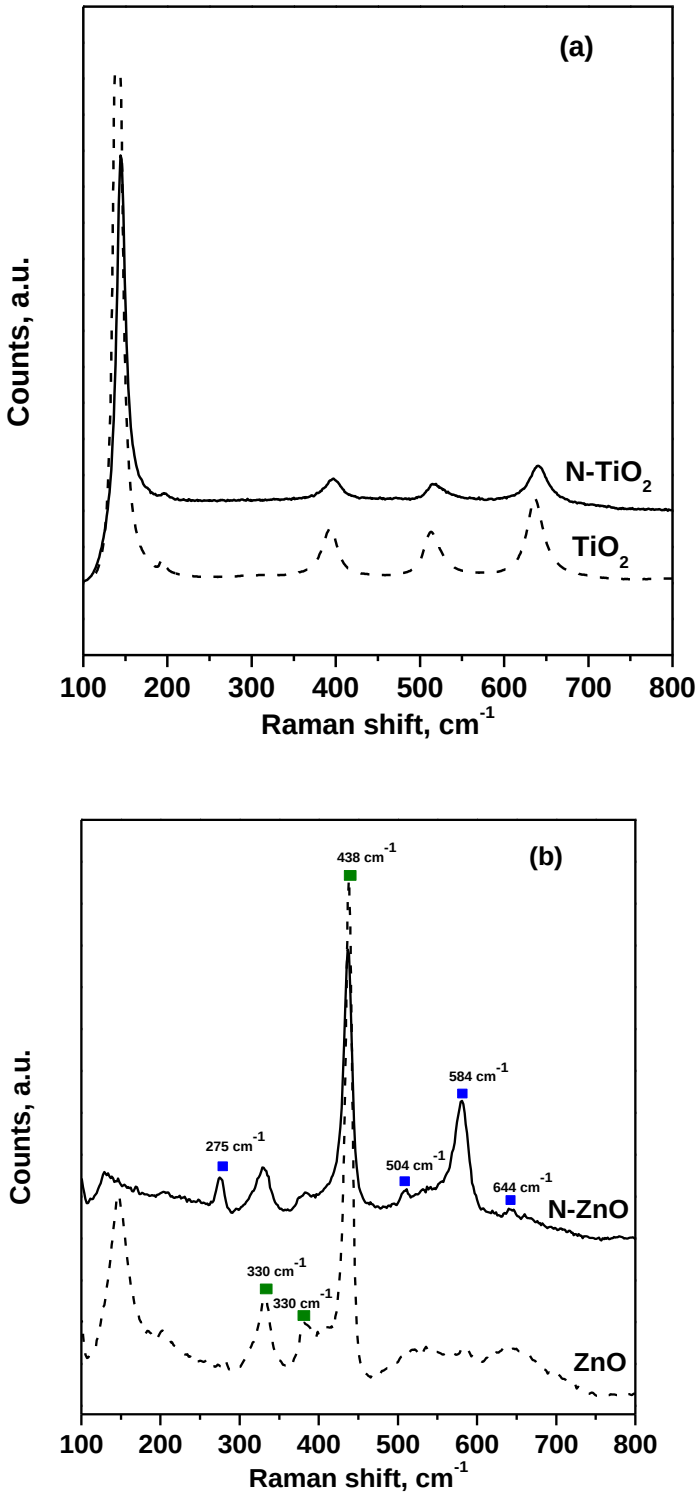

Figure 3. Raman spectra for (**a**) TiO_2 and N-TiO_2, as well as (**b**) ZnO and N-ZnO samples.

Wide-angle X-ray diffraction (WAXD) was used to identify the crystalline phase structure of all the samples (Figure 4). Figure 4a shows the spectrum of N-TiO_2 in comparison with TiO_2. The analysis demonstrates that doping with nitrogen does not change the crystalline structure of TiO_2, as all the detected patterns for both N-TiO_2 and TiO_2 can be attributed to the anatase phase (JCPS card no. 21-1272) [36]. No other phases, such as rutile and brookite, were detected, confirming the Raman spectroscopy results (Figure 3a). Figure 4b displays the WAXD patterns of ZnO and N-ZnO. All diffraction peaks were well indexed to the ZnO hexagonal wurtzite structure (JCPS Card no. 36-1451), confirming that the synthesized N-ZnO is a single-phase material. Therefore, neither doping nor synthesis method alters the phase crystallographic structure of the bare semiconductors, as demonstrated by the absence of new peaks of impurities.

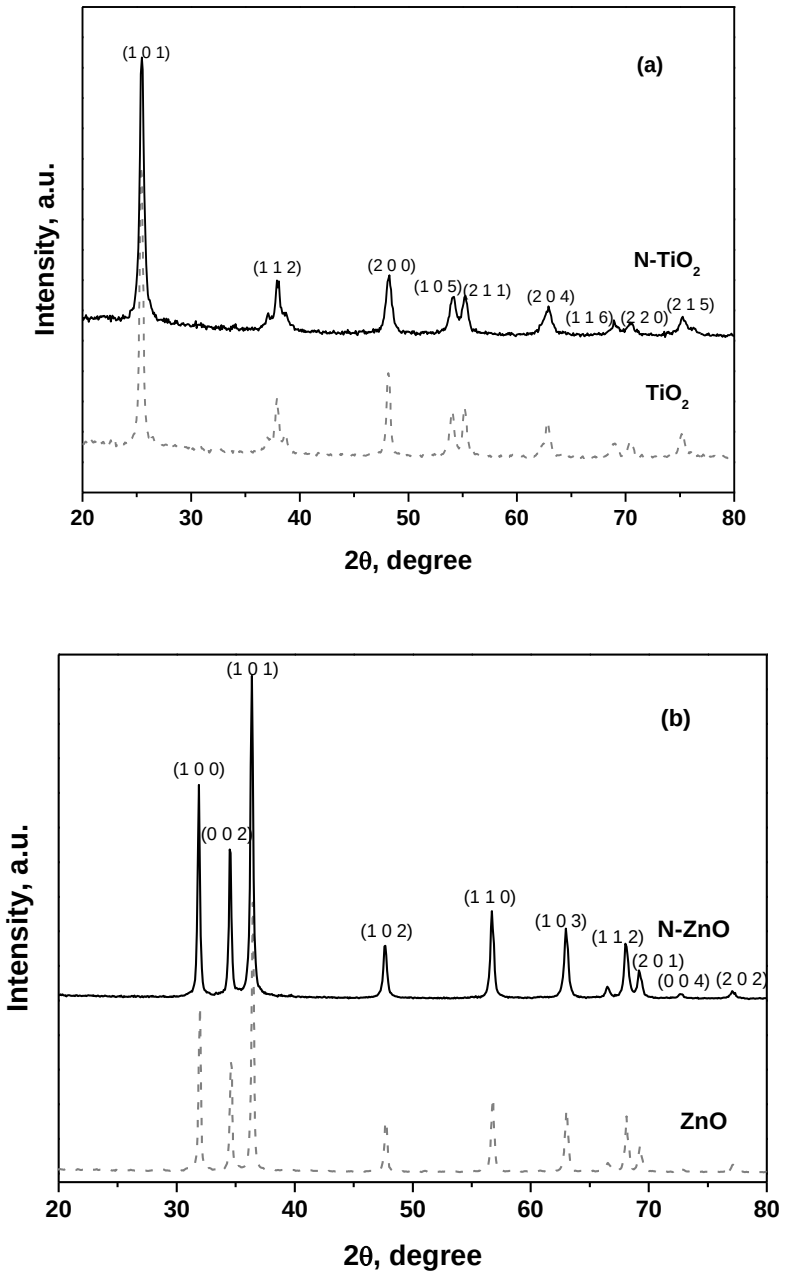

Figure 4. WAXD patterns for (**a**) TiO_2 and N-TiO_2, as well as (**b**) ZnO and N-ZnO samples in the range of 20–80°.

WAXD patterns of all photocatalysts were also examined in the 2θ range of 22–30° for TiO_2 and N-TiO_2 and in the 2θ range of 35–38° for ZnO and N-ZnO (Figure 5).

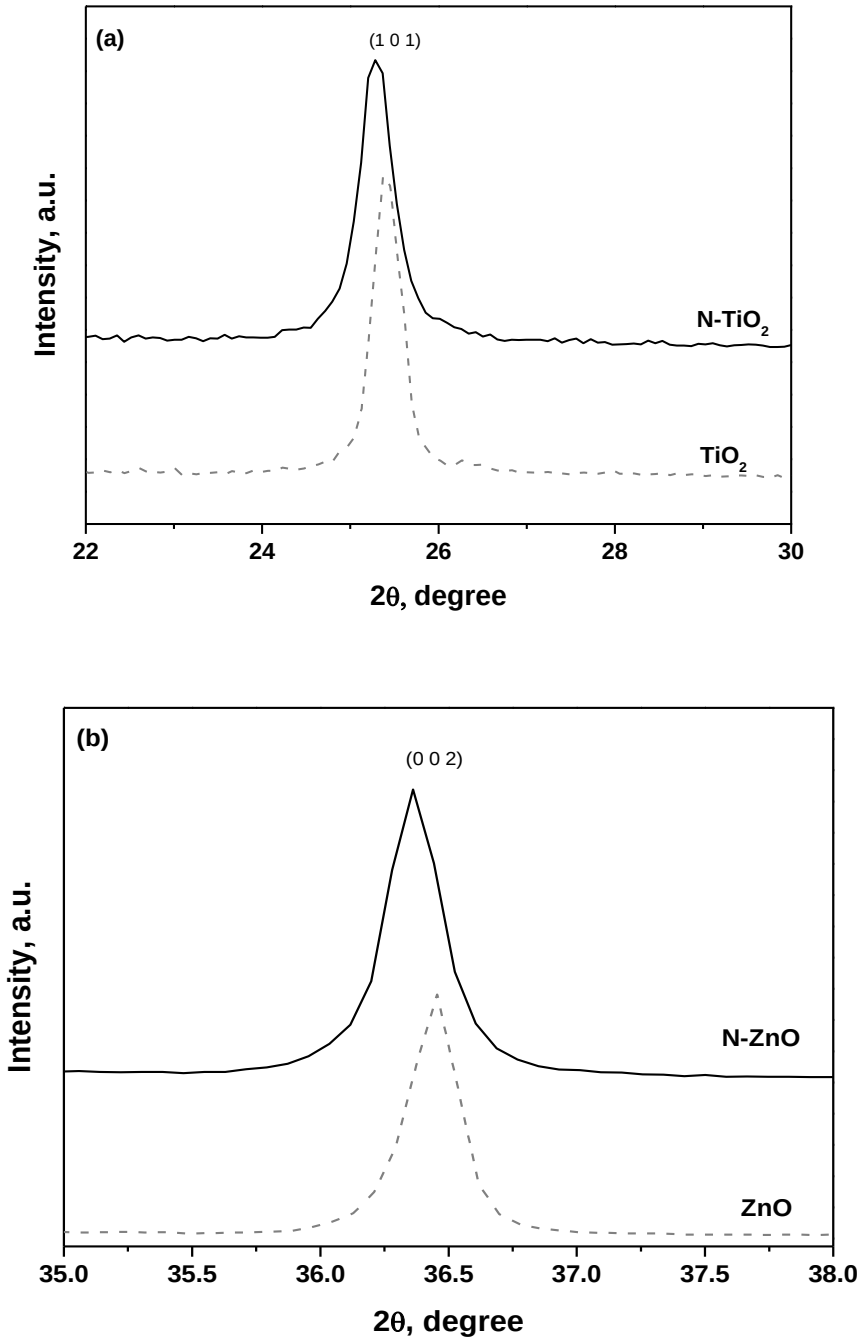

Figure 5. WAXD patterns for (**a**) TiO_2 and N-TiO_2 in the range of 22–30° and for (**b**) ZnO and N-ZnO samples in the range of 35–38°.

N-TiO_2 shows a small shift of the (101) reflection toward a lower diffraction angle (Figure 5a), indicating an enlargement of the cell parameters, which is commonly associated with the formation of an interstitial solid solution (i.e., nitrogen occupies interstitial positions in the TiO_2 lattice) [37]. N-ZnO (Figure 5b) evidences a small shift of the (002) peak toward lower angles, which is attributed to the incorporation of N at O sites, indicating that the N ionic radius (0.13 Å) is slightly larger than the O ionic radius (0.12 Å) [38,39]. The WAXD results suggest that in the case of N-TiO_2, nitrogen occupies interstitial positions, whereas for N-ZnO, some oxygen sites are replaced by nitrogen.

The average crystallite sizes of the photocatalysts were calculated using the Debye–Scherrer equation, considering the (101) reflex for titania in the anatase phase and the (100) reflex for the ZnO wurtzite phase. The obtained values are reported in Table 1.

The crystal size of TiO_2 and N-TiO_2 is almost the same, whereas in the case of N-ZnO, a slight increase was observed.

SEM analysis of N-ZnO and N-TiO_2 samples is reported in Figure S1 of Supplementary Material. N-TiO_2 is formed by particles of varying size and with a non-regular geometry, whereas N-ZnO is characterized by particles with needle-like morphology.

Table 1 reports the specific surface area (SSA) obtained by the BET method for the prepared samples. The SSA of TiO_2 slightly decreases from 50 $m^2 \cdot g^{-1}$ to 45 $m^2 \cdot g^{-1}$ after doping with nitrogen. The SSA value of ZnO and N-ZnO was equal to 5 $m^2 \cdot g^{-1}$ and 2 $m^2 \cdot g^{-1}$, respectively. Such results are in agreement with the available literature [40,41].

2.2. Photocatalytic Activity Results

Figure 6 shows the photocatalytic performances of all the samples toward EBT dye degradation under UV and visible light for TiO_2-based photocatalysts (Figure 6a) and ZnO-based photocatalysts (Figure 6b). It is important to note that the photolysis of EBT dye can be negligible under both irradiation conditions [42]. According to the curve decay observed in terms of EBT relative concentration, commercial TiO_2 and ZnO are active only under UV irradiation, reaching 56 and 100% EBT discoloration, respectively, after 180 min of irradiation time (Figure 6a,b). The photocatalytic performances of commercial TiO_2 and ZnO are extensively discussed and compared in the literature, clearly reporting that ZnO is more active than TiO_2 in the degradation of azo dyes using UV or sunlight as the excitation source [43]. It has been argued that the higher photocatalytic activity of ZnO relative to that of TiO_2 under UV light may be associated with the increased efficiency of generation and separation of photoinduced electrons and holes [44]. In particular, some authors argued that the intrinsic defects in ZnO crystal lattice are able to effectively trap the charge carriers [45,46]. In particular, Zn interstitials and oxygen vacancies (both positively charged) can enhance the photo-induced redox reactions on ZnO by trapping photo-generated electrons, therefore limiting the recombination phenomena among electrons and holes [47]. Different behavior under UV light was observed when nitrogen was inserted in the crystalline structure of both TiO_2 (Figure 6a) and ZnO (Figure 6b).

N-TiO_2 is able to absorb both UV and visible light (Figure 1a), resulting in an enhanced photocatalytic performance compared to commercial TiO_2 (Figure 6a), showing the highest photocatalytic activity under both irradiation conditions. With a fixed irradiation time, the EBT relative concentration for N-TiO_2 is lower than that observed for TiO_2, reaching a discoloration efficiency of 90% and 62% after 180 min of UV and visible light irradiation, respectively. The efficacy of the prepared N-TiO_2 was previously observed for the degradation of organic pollutants under visible light irradiation [48–50]. This might be due to interstitial nitrogen [16] (as evidenced by the WAXD analysis reported in Figure 5a), which generates intra-gap energy states above the Fermi level, causing a redshift of the N-TiO_2 absorption band edge toward the visible region [16,51]. Additionally, Di Valentin et al. underlined the beneficial contribution of oxygen vacancies to the overall visible light photoactivity of N-TiO_2 [52]. The oxygen vacancies may act as shallow donors, increasing the carrier density and facilitating the separation and transport of photo-induced carriers [53]. The possible presence of oxygen vacancies was underlined in the Raman results of N-TiO_2 sample (Figure 3a). Accordingly, the visible light activity of N-TiO_2 could be ascribed to both the presence of impurity states generated in the band gap of TiO_2 and the presence of oxygen vacancies induced by nitrogen doping [16,54].

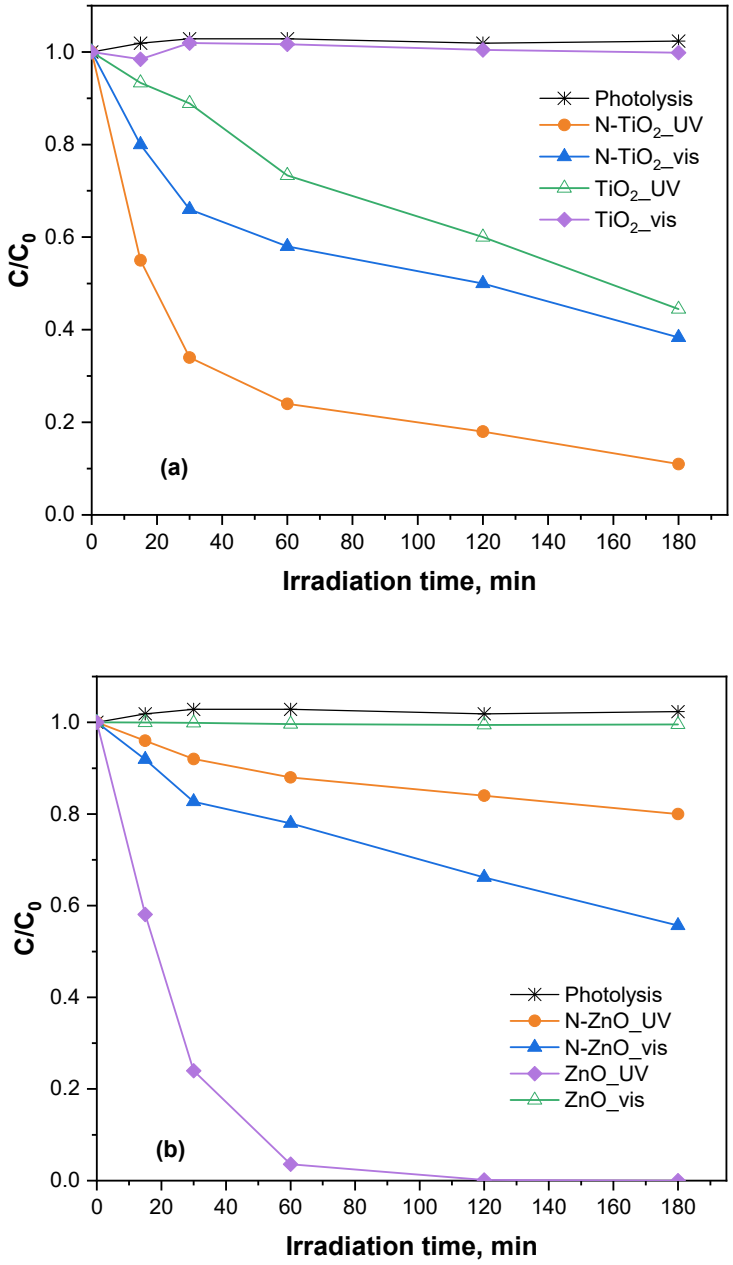

Figure 6. Photocatalytic activity under UV and visible light for (**a**) TiO_2 and N-TiO_2, as well as (**b**) ZnO and N-ZnO samples.

The N-ZnO photocatalyst showed a discoloration efficiency of about 20% under visible light and 45% under UV light (Figure 6b). Although N doping induced photoactivity under visible light, the photocatalytic efficiency of N-ZnO under UV light was significantly lower than that of undoped ZnO, in contrast to the results of the UV light test in the presence of N-TiO_2 and TiO_2 (Figure 6a).

Parhizgar et al. [55] reported that the presence of defects, such as oxygen vacancies (V_O), does not improve the photocatalytic performance of N-ZnO. Instead, the electron transfer from the donor sites (V_O) to the acceptor sites (N) determines a shift of the Fermi level toward the conduction band of ZnO, decreasing the mobility of the holes. Although the available literature [56,57] contains some reports of an enhancement in photocatalytic activity, the results in terms of EBT discoloration (Figure 6b) show that doping with nitrogen is not an efficient way to enhance the chemical reactivity of ZnO in the UV region [58]. Moreover, the achieved results could be also attributed to the concentration of N in the

ZnO lattice, which could affect the photocatalytic activity. An excess of N was observed to cover most of the surface of ZnO, inhibiting the direct exposure of the ZnO surface to the excitation light, resulting in a reduction in photocatalytic activity [59,60].

N-TiO_2 and N-ZnO photocatalysts were used for recycling experiments based on the results reported in Figure 6. Figure 7 shows five cycles of EBT photodegradation with the same sample (without any regeneration step) under visible light irradiation. The EBT discoloration of neither N-TiO_2 nor N-ZnO changed considerably for all the cycles, evidencing good stability of both photocatalysts.

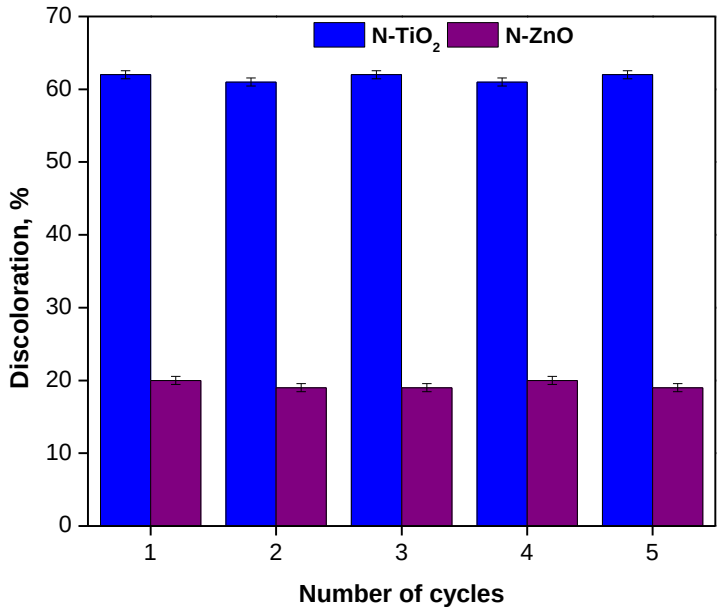

Figure 7. EBT discoloration after 180 min under visible light for five reuse cycles.

3. Materials and Methods

3.1. Preparation of N-doped Photocatalysts

Commercial anatase TiO_2 (PC50, Millennium Chemicals, Hunt Valley, MD, USA) and commercial ZnO (Aldrich, St. Louise, MO, USA) were employed as reference materials and used as received. N-doped TiO_2 (N-TiO_2) photocatalyst was prepared by sol–gel method. In detail, 25 mL of $Ti(OCH(CH_3)_2)_4$ (Aldrich, 99%) was added dropwise to 100 mL of NH_4OH solution (Carlo Erba, Val-de-Reuil, France, 30 wt%) at 0 °C under continuous stirring. The reaction involves the formation of white precipitate, which was washed with distilled water and centrifuged. The precipitate was then calcined at 450 °C for 30 min to obtain the N-TiO_2 sample. N-doped ZnO (N-ZnO) catalyst was prepared by the precipitation method starting with 0.27 g of $ZnSO_4$ (Aldrich, 99%) dissolved in 50 mL of distilled water containing 10 mL of NH_4OH solution (Carlo Erba, Val-de-Reuil, France, 28–30%). Then, NaOH solution (4 g of NaOH in 25 mL of distilled water) was slowly added at room temperature to obtain a precipitate. The generated precipitate was then centrifuged, washed, and calcined at 450 °C for 30 min to obtain the N-ZnO sample.

3.2. Photocatalyst Characterization

The ultraviolet-visible diffuse reflectance spectra (UV-Vis DRS) of the samples were recorded using a spectrophotometer (Lambda 35, Perkin Elmer, Waltham, MA, USA) equipped with an RSA-PE-20 integrating sphere for reflectance spectroscopy (Labsphere Inc., North Sutton, NH, USA). The optical band-gap values of the photocatalysts were then obtained using the Kubelka–Munk function ($F(R_\infty)$) by plotting $(F(R_\infty) * h\nu)^2$ vs. hν (eV) in the case of direct transition or by plotting $(F(R_\infty) * h\nu)^{1/2}$ vs. hν in the case of indirect transition. SEM microscopy (mod. LEO 420, Assing, Rome, Italy) was used to characterize the morphology of N-TiO_2 and N-ZnO samples at an accelerating voltage of 20 kV. The

Brunauer–Emmett–Teller (BET) surface area of the photocatalysts was determined by dynamic N_2 adsorption measurement at −196 °C with a Costech Sorptometer 1042 after pretreatment for 30 min in an He flow at 150 °C. Raman spectra were obtained with a dispersive microRaman spectrometer (Invia Renishaw, Turin, Italy) with a 541 nm laser in the range 100–800 cm^{-1}. Wide-angle X-ray diffraction (WAXD) patterns were obtained with an automatic Bruker D8 Advance diffractometer (VANTEC^{-1} detector) using reflection geometry and nickel-filtered Cu-Kα radiation.

3.3. Photocatalytic Activity Tests

Photocatalytic tests were carried out in a batch photoreactor with a cylindrical shape (ID = 2.6 cm, L = 41 cm) equipped with an air distributor device (Q_{air} = 150 $cm^3 \cdot min^{-1}$) to guarantee the presence of oxygen in the reaction medium. Four UV (main emission wavelength = 365 nm) or visible (emission wavelength in the range of 400–750 nm) lamps (Philips, Amsterdam, The Netherlands, 8 W) were placed around the external body of the photoreactor. The photocatalytic tests were conducted at room temperature using Eriochrome Black T (EBT) aqueous solution with an initial concentration equal to 100 $mg \cdot L^{-1}$, a photocatalyst dosage of 3 $g \cdot L^{-1}$, and a total volume of solution equal to 100 mL. The suspension was left in dark conditions for 120 min to achieve the adsorption/desorption equilibrium of EBT dye on the photocatalyst surface before switching on the light sources. With varying reaction times, 3 mL of the suspension was withdrawn from the photoreactor and analyzed by a UV-Vis spectrophotometer (Thermo Scientific Evolution 201, Thermo Fisher Scientific, Waltham, MA, USA) to check the reaction advancement. Before the UV-Vis analysis, the suspension was centrifuged in order to remove the photocatalyst particles. In detail, the discoloration of the chosen dye was observed by measuring the maximum absorbance value at 512 nm [61].

4. Conclusions

In this study, the properties of anatase TiO_2 and wurtzite ZnO were modified by the introduction of N-dopant into the respective lattices in order to extend the light absorption to the visible region. The presence of nitrogen in the host crystalline structure evidenced a band-gap shift to a lower value: 3.0 eV for N-ZnO and 2.35 eV for N-TiO_2. Raman spectroscopy evidenced the presence of oxygen vacancies for both N-TiO_2 and N-ZnO. In addition, WAXD analysis indicated that nitrogen occupies interstitial positions in the TiO_2 lattice, whereas in the case of N-ZnO, some oxygen sites are replaced by nitrogen. Both N-doped semiconductors evidenced an improvement in photocatalytic activity under visible light irradiation in comparison with the undoped samples, which were totally inactive. In particular, 62% and 20% EBT discoloration was achieved after 180 min for N-TiO_2 and N-ZnO, respectively. However, different behavior was observed under UV irradiation. Whereas N-TiO_2 was more photoactive than commercial undoped TiO_2, N-ZnO showed a drastic reduction in photocatalytic performance, reaching only 45% EBT discoloration compared to the total color disappearance obtained with commercial ZnO. Therefore, in order to formulate a photocatalyst at high efficiency under direct solar light, such results suggest intrinsic limitations of doping of this class of semiconductors and underline the necessity to develop a visible-light active photocatalyst by N-doping without decreasing the UV-light-driven photocatalytic performances of commercial photocatalysts.

Supplementary Materials: The following supporting information can be downloaded at: https://www.mdpi.com/article/10.3390/catal12101208/s1, Figure S1. SEM images of N-TiO_2 and N-ZnO.

Author Contributions: Conceptualization, O.S. and V.V. (Vincenzo Vaiano); methodology, O.S. and V.V. (Vincenzo Vaiano); validation, V.V. (Vincenzo Venditto); investigation, A.M., O.S. and S.P.; data curation, V.V. (Vincenzo Venditto), A.M. and S.P.; writing—original draft preparation, O.S. and A.M.; writing—review and editing, V.V. (Vincenzo Vaiano) and V.V. (Vincenzo Venditto); supervision, V.V. (Vincenzo Vaiano). All authors have read and agreed to the published version of the manuscript.

Funding: This research received no external funding.

Data Availability Statement: Not applicable.

Conflicts of Interest: The authors declare no conflict of interest.

References

1. Anpo, M. Preparation, characterization, and reactivities of highly functional titanium oxide-based photocatalysts able to operate under UV–visible light irradiation: Approaches in realizing high efficiency in the use of visible light. *Bull. Chem. Soc. Jpn.* **2004**, *77*, 1427–1442. [CrossRef]
2. Loeb, S.K.; Alvarez, P.J.; Brame, J.A.; Cates, E.L.; Choi, W.; Crittenden, J.; Dionysiou, D.D.; Li, Q.; Li-Puma, G.; Quan, X. The technology horizon for photocatalytic water treatment: Sunrise or sunset? *Environ. Sci. Technol.* **2018**, *53*, 2937–2947. [CrossRef]
3. Liu, C.; Mao, S.; Wang, H.; Wu, Y.; Wang, F.; Xia, M.; Chen, Q. Peroxymonosulfate-assisted for facilitating photocatalytic degradation performance of 2D/2D WO_3/BiOBr S-scheme heterojunction. *Chem. Eng. J.* **2022**, *430*, 132806. [CrossRef]
4. Liu, C.; Mao, S.; Shi, M.; Wang, F.; Xia, M.; Chen, Q.; Ju, X. Peroxymonosulfate activation through 2D/2D Z-scheme CoAl-LDH/BiOBr photocatalyst under visible light for ciprofloxacin degradation. *J. Hazard. Mater.* **2021**, *420*, 126613. [CrossRef]
5. Liu, C.; Mao, S.; Shi, M.; Hong, X.; Wang, D.; Wang, F.; Xia, M.; Chen, Q. Enhanced photocatalytic degradation performance of BiVO4/BiOBr through combining Fermi level alteration and oxygen defect engineering. *Chem. Eng. J.* **2022**, *449*, 137757. [CrossRef]
6. Shiraishi, Y.; Hirai, T. Selective organic transformations on titanium oxide-based photocatalysts. *J. Photochem. Photobiol. C Photochem. Rev.* **2008**, *9*, 157–170. [CrossRef]
7. Imparato, C.; Iervolino, G.; Fantauzzi, M.; Koral, C.; Macyk, W.; Kobielusz, M.; D'Errico, G.; Rea, I.; Di Girolamo, R.; De Stefano, L. Photocatalytic hydrogen evolution by co-catalyst-free TiO_2/C bulk heterostructures synthesized under mild conditions. *RSC Adv.* **2020**, *10*, 12519–12534. [CrossRef] [PubMed]
8. Iervolino, G.; Vaiano, V.; Murcia, J.; Rizzo, L.; Ventre, G.; Pepe, G.; Campiglia, P.; Hidalgo, M.; Navío, J.A.; Sannino, D. Photocatalytic hydrogen production from degradation of glucose over fluorinated and platinized TiO_2 catalysts. *J. Catal.* **2016**, *339*, 47–56. [CrossRef]
9. Vaiano, V.; Iervolino, G. Photocatalytic removal of methyl orange azo dye with simultaneous hydrogen production using Ru-modified Zno photocatalyst. *Catalysts* **2019**, *9*, 964. [CrossRef]
10. Vaiano, V.; Jaramillo-Paez, C.A.; Matarangolo, M.; Navío, J.A.; del Carmen Hidalgo, M. UV and visible-light driven photocatalytic removal of caffeine using ZnO modified with different noble metals (Pt, Ag and Au). *Mater. Res. Bull.* **2019**, *112*, 251–260. [CrossRef]
11. Franco, P.; Sacco, O.; De Marco, I.; Vaiano, V. Zinc oxide nanoparticles obtained by supercritical antisolvent precipitation for the photocatalytic degradation of crystal violet dye. *Catalysts* **2019**, *9*, 346. [CrossRef]
12. Fujishima, A.; Rao, T.N.; Tryk, D.A. Titanium dioxide photocatalysis. *J. Photochem. Photobiol. C Photochem. Rev.* **2000**, *1*, 1–21. [CrossRef]
13. Asahi, R.; Morikawa, T.; Ohwaki, T.; Aoki, K.; Taga, Y. Visible-light photocatalysis in nitrogen-doped titanium oxides. *Science* **2001**, *293*, 269–271. [CrossRef]
14. Dindar, B.; Güler, A.C. Comparison of facile synthesized N doped, B doped and undoped ZnO for the photocatalytic removal of Rhodamine B. *Environ. Nanotechnol. Monit. Manag.* **2018**, *10*, 457–466. [CrossRef]
15. Macías-Sánchez, J.; Hinojosa-Reyes, L.; Caballero-Quintero, A.d.; De La Cruz, W.; Ruiz-Ruiz, E.; Hernández-Ramírez, A.; Guzmán-Mar, J. Synthesis of nitrogen-doped ZnO by sol-Gel method: Characterization and its application on visible photocatalytic degradation of 2, 4-D and picloram herbicides. *Photochem. Photobiol. Sci.* **2015**, *14*, 536–542. [CrossRef]
16. Navarra, W.; Ritacco, I.; Sacco, O.; Caporaso, L.; Farnesi Camellone, M.; Venditto, V.; Vaiano, V. Density Functional Theory Study and Photocatalytic Activity of ZnO/N-Doped TiO_2 Heterojunctions. *J. Phys. Chem. C* **2022**, *126*, 7000–7011. [CrossRef]
17. Di Valentin, C.; Finazzi, E.; Pacchioni, G.; Selloni, A.; Livraghi, S.; Paganini, M.C.; Giamello, E. N-doped TiO_2: Theory and experiment. *Chem. Phys.* **2007**, *339*, 44–56. [CrossRef]
18. Peng, F.; Cai, L.; Huang, L.; Yu, H.; Wang, H. Preparation of nitrogen-doped titanium dioxide with visible-light photocatalytic activity using a facile hydrothermal method. *J. Phys. Chem. Solids* **2008**, *69*, 1657–1664. [CrossRef]
19. Chang, H.; Chen, G. Influence of nitrogen doping on the properties of ZnO films prepared by radio-frequency magnetron sputtering. *Thin Solid Film.* **2016**, *618*, 84–89. [CrossRef]
20. Haghighat, G.A.; Sadeghi, S.; Saghi, M.H.; Ghadiri, S.K.; Anastopoulos, I.; Giannakoudakis, D.A.; Colmenares, J.C.; Shams, M. Zeolitic imidazolate frameworks (ZIFs) of various morphologies against eriochrome black-T (EBT): Optimizing the key physicochemical features by process modeling. *Colloids Surf. A Physicochem. Eng. Asp.* **2020**, *606*, 125391. [CrossRef]
21. Jethave, G.; Fegade, U.; Rathod, R.; Pawar, J. Dye pollutants removal from waste water using metal oxide nanoparticle embedded activated carbon: An immobilization study. *J. Dispers. Sci. Technol.* **2019**, *40*, 563–573. [CrossRef]
22. Yin, S.; Liu, B.; Zhang, P.; Morikawa, T.; Yamanaka, K.-I.; Sato, T. Photocatalytic oxidation of NOx under visible LED light irradiation over nitrogen-doped titania particles with iron or platinum loading. *J. Phys. Chem. C* **2008**, *112*, 12425–12431. [CrossRef]
23. Kuroda, Y.; Mori, T.; Yagi, K.; Makihata, N.; Kawahara, Y.; Nagao, M.; Kittaka, S. Preparation of Visible-Light-Responsive $TiO_{2-x}N_x$ Photocatalyst by a Sol-Gel Method: Analysis of the Active Center on TiO_2 that Reacts with NH_3. *Langmuir* **2005**, *21*, 8026–8034. [CrossRef]

24. Cheng, B.; Shi, W.; Russell-Tanner, J.M.; Zhang, L.; Samulski, E.T. Synthesis of variable-aspect-ratio, single-crystalline ZnO nanostructures. *Inorg. Chem.* **2006**, *45*, 1208–1214. [CrossRef]
25. Surmacki, J.; Wroński, P.; Szadkowska-Nicze, M.; Abramczyk, H. Raman spectroscopy of visible-light photocatalyst–nitrogen-doped titanium dioxide generated by irradiation with electron beam. *Chem. Phys. Lett.* **2013**, *566*, 54–59. [CrossRef]
26. Samsudin, E.M.; Abd Hamid, S.B.; Juan, J.C.; Basirun, W.J.; Kandjani, A.E.; Bhargava, S.K. Controlled nitrogen insertion in titanium dioxide for optimal photocatalytic degradation of atrazine. *RSC Adv.* **2015**, *5*, 44041–44052. [CrossRef]
27. Biswas, A.; Chakraborty, A.; Jana, N.R. Nitrogen and fluorine codoped, colloidal TiO_2 nanoparticle: Tunable doping, large red-shifted band edge, visible light induced photocatalysis, and cell death. *ACS Appl. Mater. Interfaces* **2017**, *10*, 1976–1986. [CrossRef]
28. Kernazhitsky, L.; Shymanovska, V.; Gavrilko, T.; Naumov, V.; Fedorenko, L.; Kshnyakin, V.; Baran, J. Photoluminescence of Cr-doped TiO_2 induced by intense UV laser excitation. *J. Lumin.* **2015**, *166*, 253–258. [CrossRef]
29. Umar, A.; Hahn, Y. Aligned hexagonal coaxial-shaped ZnO nanocolumns on steel alloy by thermal evaporation. *Appl. Phys. Lett.* **2006**, *88*, 173120. [CrossRef]
30. Xing, Y.; Xi, Z.; Xue, Z.; Zhang, X.; Song, J.; Wang, R.; Xu, J.; Song, Y.; Zhang, S.-L.; Yu, D. Optical properties of the ZnO nanotubes synthesized via vapor phase growth. *Appl. Phys. Lett.* **2003**, *83*, 1689–1691. [CrossRef]
31. Kerr, L.L.; Li, X.; Canepa, M.; Sommer, A.J. Raman analysis of nitrogen doped ZnO. *Thin Solid Film.* **2007**, *515*, 5282–5286. [CrossRef]
32. Wang, M.; Ren, F.; Zhou, J.; Cai, G.; Cai, L.; Hu, Y.; Wang, D.; Liu, Y.; Guo, L.; Shen, S. N doping to ZnO nanorods for photoelectrochemical water splitting under visible light: Engineered impurity distribution and terraced band structure. *Sci. Rep.* **2015**, *5*, 12925. [CrossRef]
33. Das, J.; Mishra, D.; Srinivasu, V.; Sahu, D.; Roul, B. Photoluminescence and Raman studies for the confirmation of oxygen vacancies to induce ferromagnetism in Fe doped Mn: ZnO compound. *J. Magn. Magn. Mater.* **2015**, *382*, 111–116. [CrossRef]
34. Franco, P.; Navarra, W.; Sacco, O.; De Marco, I.; Mancuso, A.; Vaiano, V.; Venditto, V. Photocatalytic degradation of atrazine under visible light using Gd-doped ZnO prepared by supercritical antisolvent precipitation route. *Catal. Today* **2022**, *397*, 240–248. [CrossRef]
35. Sacco, O.; Franco, P.; De Marco, I.; Vaiano, V.; Callone, E.; Ceccato, R.; Parrino, F. Photocatalytic activity of Eu-doped ZnO prepared by supercritical antisolvent precipitation route: When defects become virtues. *J. Mater. Sci. Technol.* **2022**, *112*, 49–58. [CrossRef]
36. Li, Y.; Jiang, Y.; Peng, S.; Jiang, F. Nitrogen-doped TiO_2 modified with NH4F for efficient photocatalytic degradation of formaldehyde under blue light-emitting diodes. *J. Hazard. Mater.* **2010**, *182*, 90–96. [CrossRef]
37. Caratto, V.; Setti, L.; Campodonico, S.; Carnasciali, M.; Botter, R.; Ferretti, M. Synthesis and characterization of nitrogen-doped TiO2 nanoparticles prepared by sol–gel method. *J. Sol-Gel Sci. Technol.* **2012**, *63*, 16–22. [CrossRef]
38. Jindal, K.; Tomar, M.; Katiyar, R.; Gupta, V. N-doped ZnO thin film for development of magnetic field sensor based on surface plasmon resonance. *Opt. Lett.* **2013**, *38*, 3542–3545. [CrossRef]
39. Futsuhara, M.; Yoshioka, K.; Takai, O. Optical properties of zinc oxynitride thin films. *Thin Solid Film.* **1998**, *317*, 322–325. [CrossRef]
40. Wu, C. Facile one-step synthesis of N-doped ZnO micropolyhedrons for efficient photocatalytic degradation of formaldehyde under visible-light irradiation. *Appl. Surf. Sci.* **2014**, *319*, 237–243. [CrossRef]
41. Shifu, C.; Xuqiang, L.; Yunzhang, L.; Gengyu, C. The preparation of nitrogen-doped $TiO_{2-x}N_x$ photocatalyst coated on hollow glass microbeads. *Appl. Surf. Sci.* **2007**, *253*, 3077–3082. [CrossRef]
42. Vaiano, V.; Matarangolo, M.; Sacco, O.; Sannino, D. Photocatalytic treatment of aqueous solutions at high dye concentration using praseodymium-doped ZnO catalysts. *Appl. Catal. B Environ.* **2017**, *209*, 621–630. [CrossRef]
43. Sakthivel, S.; Neppolian, B.; Shankar, M.; Arabindoo, B.; Palanichamy, M.; Murugesan, V. Solar photocatalytic degradation of azo dye: Comparison of photocatalytic efficiency of ZnO and TiO_2. *Sol. Energy Mater. Sol. Cells* **2003**, *77*, 65–82. [CrossRef]
44. Li, Y.; Xie, W.; Hu, X.; Shen, G.; Zhou, X.; Xiang, Y.; Zhao, X.; Fang, P. Comparison of dye photodegradation and its coupling with light-to-electricity conversion over TiO_2 and ZnO. *Langmuir* **2010**, *26*, 591–597. [CrossRef]
45. Schmidt-Mende, L.; MacManus-Driscoll, J.L. ZnO–nanostructures, defects, and devices. *Mater. Today* **2007**, *10*, 40–48. [CrossRef]
46. Han, J.; Liu, Y.; Singhal, N.; Wang, L.; Gao, W. Comparative photocatalytic degradation of estrone in water by ZnO and TiO_2 under artificial UVA and solar irradiation. *Chem. Eng. J.* **2012**, *213*, 150–162. [CrossRef]
47. McCluskey, M.D.; Jokela, S. Defects in zno. *J. Appl. Phys.* **2009**, *106*, 10. [CrossRef]
48. Sacco, O.; Stoller, M.; Vaiano, V.; Ciambelli, P.; Chianese, A.; Sannino, D. Photocatalytic degradation of organic dyes under visible light on N-doped TiO_2 photocatalysts. *Int. J. Photoenergy* **2012**, *2012*, 626759. [CrossRef]
49. Jin, Y.; Zhang, S.; Xu, H.; Ma, C.; Sun, J.; Li, H.; Pei, H. Application of N-TiO_2 for visible-light photocatalytic degradation of Cylindrospermopsis raciborskii—More difficult than that for photodegradation of Microcystis aeruginosa? *Environ. Pollut.* **2019**, *245*, 642–650. [CrossRef]
50. Vaiano, V.; Sacco, O.; Sannino, D.; Ciambelli, P. Photocatalytic removal of spiramycin from wastewater under visible light with N-doped TiO_2 photocatalysts. *Chem. Eng. J.* **2015**, *261*, 3–8. [CrossRef]
51. Asahi, R.; Morikawa, T. Nitrogen complex species and its chemical nature in TiO_2 for visible-light sensitized photocatalysis. *Chem. Phys.* **2007**, *339*, 57–63. [CrossRef]

52. Di Valentin, C.; Pacchioni, G.; Selloni, A. Origin of the different photoactivity of N-doped anatase and rutile TiO_2. *Phys. Rev. B* **2004**, *70*, 085116. [CrossRef]
53. Du, S.; Lian, J.; Zhang, F. Visible light-responsive N-doped TiO_2 photocatalysis: Synthesis, characterizations, and applications. *Trans. Tianjin Univ.* **2021**, *28*, 33–52. [CrossRef]
54. Ritacco, I.; Sacco, O.; Caporaso, L.; Camellone, M.F. DFT Investigation of Substitutional and Interstitial Nitrogen-Doping Effects on a ZnO (100)–TiO_2 (101) Heterojunction. *J. Phys. Chem. C* **2022**, *126*, 3180–3193. [CrossRef]
55. Parhizgar, S.S.; Beheshtian, J. Effect of nitrogen doping on electronic and optical properties of ZnO sheet: DFT+ U study. *Comput. Condens. Matter* **2018**, *15*, 1–6. [CrossRef]
56. Mandor, H.; Amin, N.K.; Abdelwahab, O.; El-Ashtoukhy, E.-S.Z. Preparation and characterization of N-doped ZnO and N-doped TiO_2 beads for photocatalytic degradation of phenol and ammonia. *Environ. Sci. Pollut. Res.* **2022**, *29*, 56845–56862. [CrossRef]
57. Gao, J.; Zhang, X.; Sun, Y.; Zhao, Q.; Yu, D. Compensation mechanism in N-doped ZnO nanowires. *Nanotechnology* **2010**, *21*, 245703. [CrossRef]
58. Elias, M.; Uddin, M.N.; Saha, J.K.; Hossain, M.A.; Sarker, D.R.; Akter, S.; Siddiquey, I.A.; Uddin, J. A highly efficient and stable photocatalyst; N-doped ZnO/CNT composite thin film synthesized via simple sol-gel drop coating method. *Molecules* **2021**, *26*, 1470. [CrossRef] [PubMed]
59. Shinde, S.; Bhosale, C.; Rajpure, K. Photocatalytic degradation of toluene using sprayed N-doped ZnO thin films in aqueous suspension. *J. Photochem. Photobiol. B Biol.* **2012**, *113*, 70–77. [CrossRef]
60. Kumari, V.; Mittal, A.; Jindal, J.; Yadav, S.; Kumar, N. S-, N-and C-doped ZnO as semiconductor photocatalysts: A review. *Front. Mater. Sci.* **2019**, *13*, 1–22. [CrossRef]
61. Sacco, O.; Vaiano, V.; Navarra, W.; Daniel, C.; Pragliola, S.; Venditto, V. Catalytic system based on recyclable Fe0 and ZnS semiconductor for UV-promoted degradation of chlorinated organic compounds. *Sep. Purif. Technol.* **2021**, *270*, 118830. [CrossRef]